

1 **Abstract**

2 By means of a newly designed portable aerosol mass spectrometer SPLAT (**S**ingle **P**article **L**aser
3 **A**blation **T**ime-of-flight mass spectrometer) for the analysis of single atmospheric aerosol particles we
4 investigated the system performance in dependency of two different aerodynamic lenses (Schreiner and
5 Liu type) capable of focusing particles with diameters ranging from 80 nm to 800 nm and 300 nm to
6 3000 nm, respectively. By using the pressure regulated Schreiner lens, the instrument is independent of
7 variations in atmospheric pressure which would lead to changing dynamical properties of the aerosol
8 particles. Active pressure control inside the inlet system facilitates airborne measurements without
9 complicated corrections. With the Liu setup no pressure regulation was used. Here the overall
10 efficiency of our instrument is 7% while with the Schreiner setup 2% was achieved. The Liu lens setup
11 is optimal for measuring submicron particles at low particle concentrations. To detect supermicron
12 particles the Schreiner lens setup is favored. Together with these experiments we present details of the
13 setup, its characterization, laboratory studies as well as preliminary results of a field campaign for the
14 analysis of atmospheric aerosol particles. Our instrument is able to measure simultaneously the size and
15 the chemical composition of single aerosol particles larger than 300 nm in diameter. It uses forward
16 scattered light of single aerosol particles at two positions to determine their aerodynamic size from the
17 flight time between the two lasers. Chemical analysis of the particles is done by laser ablation mass
18 spectrometry utilizing a bipolar time-of-flight mass spectrometer.

1 **Introduction**

2 On-line mass spectrometry for the chemical analysis of aerosols has become an important instrument in
3 atmospheric research (Nash et al. 2006). One of the major issues connected with particle mass
4 spectrometers is the design of suitable sampling inlets. Such inlets need to provide sufficient particle
5 numbers for analysis inside the vacuum cell as well as permit entrance of the size range covered by the
6 detection method. For mass spectrometric chemical particle analyses two main approaches are
7 distinguished, each of which requires specific inlet designs: I.) thermal vaporization of aerosol
8 ensembles with subsequent electron impact ionization (EI) and mass separation by time-of-flight (TOF)
9 or a quadrupole (Canagaratna et al. 2007), described in the literature as Aerosol Mass Spectrometer
10 (AMS) and II.) vaporization and ionization with a laser pulse and mass separation by a TOF-MS
11 (Murphy et al. (2007)).

12 The former technique generally analyzes aerosol ensembles and generates quantitative data but only of
13 material which is vaporized at temperatures up to 600°C. With the latter technique single particles are
14 analyzed. In practice the instruments of type I are designed for particles with sizes from a few tens of
15 nanometers to roughly 1 micron while those of type II commonly detect particles from >100 nm to a
16 few microns. Already from this difference the need for specific inlet designs arises. Laser
17 desorption/ionization (LDI) enables the detection of refractory material and therefore complements
18 AMS measurements.

19 However, in LDI for equal particles, signal intensities are varying from particle to particle, so
20 quantitative results cannot be drawn. A molecular dynamics modeling study of the particle ablation
21 process is presented by Schoolcraft et al. (2000) which shows that particle disintegration depends on
22 the particle size, transparency of the particle components at the ablation wavelength and laser fluences.
23 Even for small particles at low laser fluences a significant number of molecules remain bound in large
24 clusters, which are not analyzed.

1 Besides a commercial instrument (ATOFMS, Aerosol Time-of-flight Mass Spectrometer, TSI Inc.)
2 which is based on the instrument developed by Prather and co-workers (Gard et al. (1997), Su et al.
3 (2004)), several other home-build single particle mass spectrometers exist. All of these instruments
4 differ in some details, for example the wavelength of the ionization laser, the inlet, the TOF setup, etc.,
5 but the working principle is the same. The particles enter the system through an inlet; in most systems
6 in these days an aerodynamic lens is preferred over a capillary inlet because of its much higher
7 focusing ability (Cziczo et al. (2003)). Field measurements by Schneider et al. (2004) also
8 demonstrated the need for higher sampling efficiencies than inherent in capillary designs when data
9 under real atmospheric conditions are to be gathered.

10 The aerodynamic lens allows focusing of the particles into a narrow particle beam by use of a sequence
11 of several orifices. Different aerodynamic lenses are used and described in the literature. The
12 commercial ATOFMS is equipped with a critical orifice with a diameter of 110 μm and a series of five
13 orifices (5.0 mm; 4.8 mm; 4.5 mm; 4.3 mm; 4.0 mm, Su et al. (2004)). The setup for the SPLAT-MS
14 by Imre (Single Particle Laser Ablation Time-of-flight Mass Spectrometer) is similar using a 100 μm
15 critical orifice followed by six apertures with decreasing diameter from 5.0 mm to 3.0 mm (Zelenyuk
16 and Imre (2005)). This kind of lens design (Liu et al. (2007)) is also used for the Aerodyne Aerosol
17 Mass Spectrometer (AMS) with thermal vaporization and EI ionization.

18 Another lens design which is used by the aircraft based version of the PALMS instrument (Particle
19 Analysis by Laser Mass Spectrometry, Thomson et al. (2000)) is based on the work of Schreiner et al.
20 (1999). Here a series of seven orifices with decreasing diameter from 1.4 mm to 0.25 mm is deployed.
21 The lens works at pressures from 15 mbar to 200 mbar, which is much higher compared to the Liu
22 design operating at 1 mbar to 2 mbar. Because pressures in the 15 mbar to 200 mbar regime can be
23 regulated very easily, a pressure control was implemented with the Schreiner lens design. The
24 performance of the lens is therefore not affected by changes in ambient pressure which is a prerequisite

1 for aircraft based systems. Cziczo et al. (2004) present a study on cirrus ice residue using the Schreiner
2 type isobaric lens as an inlet for the PALMS onboard of the NASA WB-57F.

3 The lens system designed by Liu was also deployed in aircraft based measurements with the Aerosol
4 Mass Spectrometer (Kleimann et al. (2007), Schneider et al. (2006), Bahreini et al. (2003), DeCarlo et
5 al. (2006)). The pressure at the inlet of the aerodynamic lens is determined by a critical orifice (100 μm
6 in diameter for most AMS systems) and it is not actively pressure controlled. Therefore, corrections
7 have to be applied when this lens setup is used at variable pressure conditions, which is described in
8 detail by Bahreini et al. (2003) and Schneider et al. (2006).

9 The working principle of both lens setups is the same. Inside the aerodynamic lens small particles are
10 accelerated to higher velocities than large particles. In most single particle mass spectrometers the
11 particles in the particle beam are detected at two positions by means of light scattering. For each single
12 particle its aerodynamic diameter is derived and the appropriate time to fire an intense laser pulse for
13 particle ablation is calculated from the time interval between the two scattering signals. The resulting
14 ions are mass analyzed. To get a complete picture of the chemical composition of individual particles,
15 usually bipolar TOF mass spectrometers are deployed.

16 The purpose of this paper is to provide a laboratory characterization of the key parameters of the two
17 lens designs (Schreiner and Liu type) when used as inlets for laser ablation instruments. The instrument
18 equipped with the Schreiner type lens operates independent of ambient pressure. Using the Liu type
19 lens, the instrument performance is affected by ambient pressure variations because it is not actively
20 controlled with a valve and pump. Also details of the newly developed SPLAT instrument are
21 presented together with preliminary results from the first campaign in which our instrument was
22 involved.

23

1 **Instrument Description**

2 A sketch of the SPLAT instrument is shown in the upper part of Figure 1. The system consists of three
3 main parts (I – III), which are marked in the Figure. The aerosol particles are introduced into the
4 instrument and focused onto a narrow particle beam by the aerodynamic lens (I). In the main vacuum
5 chamber, the particles are detected by measuring the light scattered by single particles crossing two
6 continuous laser beams (II). The time-of-flight between the two laser foci is used to determine the
7 particle size and to trigger a pulsed laser which vaporizes the particle and ionizes the particle vapor
8 (III). The resulting ions are detected by a bipolar time-of-flight mass spectrometer, which allows a
9 detailed analysis of the chemical composition of the individual aerosol particle.

10 The whole instrument is built in a rack with dimensions of 140 cm x 100 cm x 51 cm and weighs about
11 250 kg. Except for the ionizing laser, computer, monitor and roughing pump everything is powered
12 with a 28 V supply and subsequent power conversion to 24 V and 48 V. During measurements the
13 instrument has a current consumption of 6.7 A at 28 V. With these specifications the instrument is well
14 suited for deployment in the field and on mobile platforms such as ships, vans and research aircraft.

15

16 **Inlet (I) and Vacuum System**

17 The particles enter the instrument through an aerodynamic lens of the Schreiner or the Liu type and are
18 focused into a narrow beam. The Schreiner lens type was designed by J. Schreiner at the MPI for
19 Nuclear Physics (Schreiner et al. (1999)). The lens consists of 7 apertures, which are mounted in a
20 107 mm long stainless steel tube with an inner diameter of 6.0 mm. The apertures with a thickness of
21 0.2 mm have decreasing inner diameters from the inlet to the outlet of the lens from 1.3 mm to
22 0.65 mm and are separated by 13 mm long spacers with inner diameters from 3.5 mm to 2.0 mm. In
23 addition to the 7 apertures, as an accelerating orifice, a 0.25 mm aperture is used at the exit of the
24 aerodynamic lens. A schematic drawing of the lens is presented in the lower part of Figure 2.

1 A 250 μm orifice mounted in front of the lens with a distance of 24 mm is typically used to regulate the
2 flow into the lens. Different volumetric flows can be realized by choosing different critical orifices
3 (100 μm - 250 μm cf. Table 1). The pressure behind the critical orifice in the pre-vacuum chamber (1)
4 and thus in front of the aerodynamic lens is adjustable. A pressure controller (Bronckhorst, El-Press,
5 P502C-FBB-022A) together with a scroll pump (Varian, SH-100) which also serves as the fore pump
6 for all turbo molecular pumps allows the regulation of the pressure from 50 mbar to 250 mbar at the
7 inlet of the aerodynamic lens. By using this pressure regulation, the instrument is independent of
8 variations in atmospheric pressure which would otherwise lead to changing aerodynamic properties and
9 therefore variations in the flight path and the focusing of the aerosol particles. This independency of the
10 lens performance on pressure variation is a prerequisite for aircraft measurements.

11 Alternatively to the above described lens, which focuses particles in the size diameter range of 300 nm
12 to 3000 nm and is not affected by variations in ambient pressure, the aerodynamic lens with the Liu
13 design was also integrated in the SPLAT instrument for the purpose of comparing the detection
14 efficiency. This efficiency is influenced by the cross section of the particle beam and the detection laser
15 beam and hence a function of particle beam width. The Liu lens focuses particles in the size range from
16 ~ 80 nm to ~ 800 nm. The flow rate of $76 \text{ cm}^3/\text{min}$ into the lens is regulated by a 100 μm critical orifice.
17 The pressure behind the critical orifice at the inlet of the aerodynamic lens is 1.6 mbar at ambient
18 conditions. The lens consists of 6 apertures with decreasing diameters from 5.0 mm to 3.0 mm. The
19 apertures in a 180 mm long stainless steel tube with an inner diameter of 10.3 mm are separated by
20 29 mm spacers with an inner diameter of 9.5 mm. A schematic drawing of the lens can be found in the
21 upper part of Figure 2.

22 For a successful operation of the instrument, a precise adjustment of the particle beam to the foci of the
23 detection and ionization lasers is indispensable. The aerodynamic lens is mounted in a flange, which
24 allows tilting and shifting of the whole lens by means of a set of micrometer screws. Therefore it is

1 possible to adjust the position and the direction of the particle beam in the vacuum chamber with a
2 precision of a few micrometers. In operation, the chamber at the exit of the aerodynamic lens is
3 pumped down to 10^{-1} mbar by two turbo molecular pumps (Adixen, ATH31+) (pump 2 in Figure 1). A
4 skimmer with an opening diameter of 1.0 mm separates the first pumping stage from the main vacuum
5 chamber and the two mass spectrometer flight tubes, in which the pressure is reduced down to 10^{-6}
6 mbar by two turbo molecular pumps (Pfeiffer Vacuum, TMH 261 U-P) (pump 3 in Figure 1).

7

8 **Sizing of Particles (II) and Size Calibration**

9 The aerodynamic size of the aerosol particles is determined by the flight time of the particles between
10 two sizing laser beams with a distance of 29 mm. The position of the first detection laser beam is
11 located 47 mm behind the exit of the aerodynamic lens. A green diode pumped solid state Nd:YAG cw-
12 laser (Coherent, compass 315M-150) with a wavelength of 532 nm is coupled into a glass fiber, where
13 the beam is divided into two laser beams by a fiber optic beam splitter (OZ-Optics, Fused-12-532-
14 3.5/125-50/50-3AF1A1A-3-0.5). The laser output power of 150 mW is coupled into the fiber with an
15 efficiency of 70%, so at the end of each fiber optic line a power of 52 mW is available. The ends of the
16 two fiber optic lines are fixed on xy-micro tables (Owis, MKT 40C XY), which are mounted directly at
17 the outside of the vacuum chamber. The xy-tables allow an accurate adjustment of the detection laser
18 foci with a spatial precision of 1 μm in both dimensions perpendicular to particle beam propagation.
19 Therefore the distance between the two laser foci remains constant. Each laser beam is focused to a
20 diameter of $\sim 190 \mu\text{m}$ ($1/e^2$) by a grin lens, located at the end of the optical fiber, with a focal distance
21 of 85 mm.

22 The two detection laser beams, separated by a distance of 29 mm, are orientated orthogonal to each
23 other and both orthogonal to the propagation direction of the particle beam. When an aerosol particle
24 crosses the laser focus, the generated scattered light is imaged with two plano convex lenses (Topag, f

1 = 23 mm) onto a photomultiplier (Hamamatsu, R1463) with a maximum gain of 10^6 . A schematic
2 drawing of the optical detection setup is presented in the lower part of Figure 1. To minimize the
3 background radiation a spatial filter with an opening diameter of 200 μm is placed at the focal point of
4 the second lens in front of the multiplier. The scattered light is collected in forward direction under an
5 angle of $\sim 5^\circ$ to $\sim 24^\circ$, whereas the direct laser beam (0° to $\sim 5^\circ$) is captured in a beam stop which is a
6 black anodized cup. Further reduction of the background radiation is achieved by using windows with
7 antireflection coatings for 532 nm.

8 The signal from the multiplier is amplified with custom build preamplifiers resulting in ~ 90 mV
9 signals for 300 nm particles with a background signal of ~ 70 mV. Further handling of the light
10 scattering signals is done on a custom build electronic card which applies a discriminator to the signals
11 and measures the time between the two signals. Because the preamplifiers are saturated at 900 mV by
12 light scattering signals resulting from particles larger than 800 nm the light scattering intensity can not
13 be used for evaluating the particle size beyond this diameter.

14 The transit time of the particles between the two foci of the detection laser, which is typically in the
15 order of 150 μs , is used to obtain the aerodynamic size with a resolution of 50 ns. Only flight times that
16 correspond to reasonable particle sizes are used for further processing. The actual processing rate is
17 5 Hz. Calibration measurements for the sizing procedure are performed with standardized particles.

18 The flight times of Polystyrene latex (PSL) particles in the size range from 300 nm up to 3.0 μm are
19 measured and fitted to their vacuum aerodynamic size using a second order polynomial, which is then
20 used for calculating the size of unknown particles. Typically correlation coefficients better than 0.999
21 are obtained.

22

23 **Ablation of Particles (III) and Chemical Analysis by TOF-MS**

24 At a distance of 105 mm behind the exit of the aerodynamic lens, an ArF excimer laser (Lambda

1 Physik, Optex) with a wavelength of 193 nm, pulse duration of 8 ns and maximum pulse energy of
2 13 mJ/pulse evaporates the aerosol particle at least partially and ionizes molecules in the resulting
3 vapor within a single laser pulse. Typically pulse energies of 6-8 mJ/pulse are used in the constant
4 energy mode of the laser. The maximum repetition rate of the laser is 200 Hz which is by far enough
5 compared to the maximum repetition rate of the detection system of 5 Hz. The gas filling of the laser
6 has to be replaced after some 100 000 laser shots due to insufficient pulse energy. The laser beam is
7 focused with a lens (Linos photonics, $f = 272$ mm) to a spot size of $\sim 250 \mu\text{m} \times 500 \mu\text{m}$ resulting in
8 maximum energy densities of $\sim 1.6 \cdot 10^9 \text{ W/cm}^2$. The focus is aligned with the wider dimension parallel
9 to the particle beam. With a mean particle velocity of 200 m/s the particles need approximately $2.5 \mu\text{s}$
10 to travel through the laser focus. The measured particle transit time between the two detection laser foci
11 is used to determine the arrival time of the particles in the ionization region, which is located 29 mm
12 behind the second detection laser beam with a precision of 50 ns.

13 The ions created by the laser ablation process are extracted by electrodes with Wiley-McLaren type
14 geometry into two time-of-flight mass spectrometers (RM Jordan Inc.). The electrodes have a diameter
15 of 28.5 mm with an opening diameter of 18.5 mm which is covered with a copper grid (transmission
16 88%) to generate a homogeneous electrical field in the ion source. The distance between the two
17 accelerating grids is 8.5 mm with ± 1500 V applied to the grids, resulting in an accelerating field of
18 3530 V/cm.

19 Both spectrometers are equipped with reflectrons to enhance the mass resolution of the mass spectra.
20 The field free flight path for the ions is 745 mm. A microchannelplate-detector (MCP) with two
21 microchannelplates (25 mm diameter, L/D 40:1) in chevron configuration (Scientific Instruments, S25-
22 10-D) measures a time-depended current due to the varying flight times of ions with different m/z
23 ratios. The cationic MCP signal is terminated with 50 ohm and directly analyzed with a digitizer card, a
24 digital 8 bit oscilloscope-card (Acqiris, DC 240) with two input channels and a maximal sampling rate

1 of 2 GS/s. The anionic MCP signal which is generated at ~ 4000 V has to be decoupled with a
2 capacitor.

3

4 **Alignment Procedure**

5 To obtain high detection efficiencies a special alignment sequence was developed. First for every
6 detection stage, the detection laser beam is centered with two alignment apertures to ensure that the
7 detection laser beam is located in the middle of the beam stop and the spatial filter is arranged on the
8 same optical axis. Then, the aerodynamic lens is tilted in the direction perpendicular to the detection
9 laser beam. For every position the number of light scattering signals is averaged over three 10s time
10 periods. For both detection stages the resulting particle beam profile is fitted with a Gaussian profile
11 and the maximum is determined. In that way the cross sections of the particle beam with the two
12 detection laser beams is maximized. To increase the signal to noise ratio further, the position of the
13 spatial filter on the optical axis is optimized.

14 After the position of the particle beam is fixed, the excimer laser beam has to be aligned to find the
15 optimal cross section between the particle beam and the excimer laser beam. The screening of the cross
16 section has to be performed in two dimensions, one dimension perpendicular to the particle beam and
17 in direction of the excimer laser beam, the other in direction of particle beam propagation. The first is
18 altered with a micrometer screw. The second corresponds to a change in the trigger delay of the
19 excimer laser. To find the best position for the excimer laser beam, the hit rate, which is defined as the
20 ratio of the number of sized particles to that of the particles successfully hit by the excimer laser beam,
21 for 100 sized particles is determined on this two-dimensional surface.

22

23 **Process Control and Data Acquisition**

24 The SPLAT instrument is set up as a field instrument and therefore it is designed to work reliably with

1 minimum operational and supervision effort for the user. The instrument is able to automatically handle
2 interruptions in power supply, leaks in the vacuum system or pump failures. The process control of the
3 instrument is separated from the data acquisition. All turbo molecular pumps, the high voltage supply,
4 pressure regulation at the inlet of the aerodynamic lens, acquisition of housekeeping data and the
5 particle detection system are managed by an embedded controller system (MME Müller
6 Mikroelektronik). The temperature, the rotation speed and the power consumption of the turbo
7 molecular pumps, the pressures at the inlet of the aerodynamic lens and at the two flight tubes are sent
8 via a serial port to a PC. These data are stored in a separate file every 10 minutes. When the pressure in
9 the flight tubes exceeds the typical operational pressure of $3 \cdot 10^{-6}$ mbar the system automatically turns
10 off the high voltage supplies and all turbo molecular pumps.

11 Handling of the light scattering signals is performed with a custom build trigger card. To discriminate
12 the background from the light scattering signals a threshold can be set separately for both detection
13 stages. The time between the two signals is measured in frequency time steps (50 ns) of the trigger card
14 processor with a certain slope. The same time but with an adjustable slope is used to send the trigger
15 signal to the excimer laser. The ratio of the two slopes specifies the trigger delay for the excimer laser.
16 The number of time steps and the intensity of both light scattering signals are stored together with the
17 exact date and time (0.1 s resolution) in a separate file. The number of time steps is also stored together
18 with the mass spectra of a particle. Currently, the maximum data recording rate is 5 Hz which is limited
19 by processing the scattered light signals.

20 Mass spectra for both polarities are recorded with an 8 bit digitizer card. A $40 \mu\text{s}$ time interval is
21 recorded with 2 ns resolution, resulting in 20000 points for each polarity and particle. A maximum
22 time-of-flight of $40 \mu\text{s}$ corresponds to a maximum m/z of 424 for cations and 366 for anions. Mass
23 spectra are stored in 8 bit data format, resulting in 44 kB files for each single particle. Time to mass
24 conversion is performed by use of calibration measurements of known substances with a linear relation

1 between the time-of-flight and the square root of the m/z value.

2 A new calibration is performed when the voltages of the mass spectrometer or the position of the
3 excimer laser are changed. A refinement of mass calibration factors by internal calibration is optional
4 for every spectrum with two or more peaks. The algorithm for refining mass calibration factors is
5 described by Haas and Kalcher (1996). To be accepted as new, the mass calibration factors have to be
6 within 10% and 20% of the old values for slope and intercept, respectively. With this procedure, errors
7 in mass assignment due to excess energy during the ablation process can be minimized, but it is
8 currently not possible to work with an accuracy higher than integer masses.

9 The resulting mass calibration factors are used to integrate the spectrum over integer masses and thus
10 “stick spectra” are generated. The integration is carried out for the cationic and anionic spectrum up to
11 m/z 220 which generates a vector with 440 elements for each particle. In the cationic as well as in the
12 anionic mass spectra generally no signals are found for masses higher than m/z 220. The vectors are
13 normalized for cations and anions separately and stored consecutively in a matrix which is used for
14 further analysis using a classification algorithm. By applying the normalization, information about the
15 absolute intensity is lost, but this information is not necessary for subsequent analysis because in
16 classification algorithms the structure of the peak progression and not the absolute intensity is used.

17 The software for data acquisition and data preprocessing is written as Labview program code (National
18 Instruments).

19

20 **Experimental Setup for Measurements of Detection Efficiency**

21 An aerosol of polystyrene latex (PSL) particles (Duke Scientific) with variable diameters from 300 nm
22 to 3000 nm is generated with a constant output atomizer (TSI, Model 3076) and dried by a diffusion
23 drier filled with silica gel. From 300 nm to 800 nm the aerosol is size-selected with a differential
24 mobility analyzer DMA (TSI, Model 3080). The concentration is measured with a condensation

1 particle counter CPC (TSI, Model 3025A). For PSL particles from 800 nm to 3000 nm there is no size-
2 selection with a DMA and the concentration is measured with an optical particle counter OPC (Grimm,
3 Model 1.108) or an aerodynamic particle sizer APS (TSI, Model 3321). At 800 nm all three methods of
4 calibration can be compared. Typical concentrations for the monodisperse aerosol were 10 to 20 #/cm³,
5 which results in detection rates far below the 5 Hz limit for the detection system.

6 In this paper we define the detection efficiency as the product of the optical detection efficiency, the
7 transmission of the lens and an enrichment factor for the inlet system. The optical detection efficiency
8 is the fraction of the number of particles which are sized compared to the number of particles which
9 enter the sizing region. The transmission of the lens is the fraction of the particles exiting from the lens
10 compared to those which entered the lens. The enrichment factor is only defined for the actively
11 pumped Schreiner lens. Here the particles enter the lens through a critical orifice with 250 μm diameter
12 which results in a flow rate of 518 cm³/min at ambient pressure. Behind the orifice the pressure is
13 reduced to a value between 50 mbar and 250 mbar by active pressure control. The flow rate through the
14 aerodynamic lens (398 cm³/min) is measured at the lens entrance. If the particles are pumped away
15 with the same ratio as the air, the enrichment factor is 1. The maximum enrichment factor is 20 if we
16 assume that all trajectories of the particles which enter the instrument through the critical orifice end in
17 the entrance of the lens and are not influenced by the air trajectories. For the Liu lens the enrichment
18 factor is one because it is not actively pumped. It is not possible to give individual values for the
19 enrichment factor, the transmission of the lens and the optical detection efficiency, but the detection
20 efficiency can be measured and compared with those of other single particle mass spectrometers.

21

22 **Instrument Characterization**

23 **Particle Size Measurement**

1 For the Liu lens design Knudsen numbers (Kn) are between 1025 and 102.5 for particles in the size
2 diameter range of 80 nm to 800 nm at 1.6 mbar and particle acceleration takes place in the free
3 molecular regime ($Kn > 10$). Therefore particle sizes are defined as vacuum aerodynamic diameters
4 (d_{va}) and calculations have to be performed according to DeCarlo et al. (2004). For the Schreiner lens
5 design (particles with diameters between 300 nm and 3000 nm at 50 mbar to 250 mbar) Kn values are
6 between 8.7 and 0.87, so particle acceleration takes place in the transition regime ($0.1 < Kn < 10$).
7 However, calculations for the Schreiner lens design are also performed with the vacuum aerodynamic
8 diameter to have better comparability. The maximum error is the square root of the density, which is
9 1.025 for PSL particles (density 1.05 g/cm^3).

10 The SPLAT instrument determines the vacuum aerodynamic diameter of a particle by measuring the
11 transit time between the foci of the two detection lasers. To calculate the diameter from the flight time,
12 various calibration measurements with standard materials have to be carried out. The flight time is
13 fitted with a quadratic function to the vacuum aerodynamic diameter. A size distribution of PSL
14 particles with 10 different diameters ranging from $0.4 \mu\text{m}$ to $3.0 \mu\text{m}$ at a pressure of 90 mbar at the
15 entrance of the aerodynamic lens (Schreiner type) is shown in Figure 3. The different sizes are clearly
16 separated. The vacuum aerodynamic diameters for the PSL particles calculated from the quadratic fit
17 are listed in Table 2. The standard deviation from a Gaussian fit to the size distributions are given as
18 uncertainties.

19 Figure 4 shows a size distribution for various PSL particles in the size range from 300 nm to 800 nm,
20 focused with the Liu lens. Although the Liu lens has a high transmission for particles in the size range
21 between 80 nm and 800 nm (Liu et al. (2007)), calibrations with particles smaller than 300 nm are not
22 possible because in our setup the light scattering detection becomes inefficient. The vacuum
23 aerodynamic diameters calculated from the calibration for the Liu lens design are presented together
24 with the standard deviations in Table 2. Similar to the Schreiner lens setup the Liu lens setup provides

1 clearly separated size distributions for the different particles sizes. The uncertainties derived from the
2 Gaussian fit of the different size modes are similar to those from the Schreiner lens setup and both are
3 close to the manufacturers specifications. If it is assumed that the largest instrumental source of
4 uncertainty is the duration of the light scattering pulse compared to the flight time between the two
5 detection lasers, a relative error of the size measurement of 0.66% can be calculated which is not size
6 dependent. This value is smaller compared to the relative width of the measured size distributions,
7 found to be between 2.1% and 0.7%. Therefore the uncertainty of the size measurements with the
8 SPLAT instrument is determined by the uncertainty in the size distribution of the PSL particles.

9 Because particle acceleration in the last aperture of the lens and therefore the transit time through the
10 detection laser setup is dependent on the pressure in the aerodynamic lens, particle size calibrations
11 have been carried out for pressures in the range of 50 mbar to 250 mbar to cover the whole adjustable
12 pressure range of the Schreiner lens. Figure 5 shows the relationship between particle time-of-flight
13 and particle vacuum aerodynamic diameter for seven different pressures at the inlet of the Schreiner
14 lens. For each pressure there is a satisfactory quadratic dependence between particle time-of-flight and
15 particle vacuum aerodynamic diameter. With increasing pressure at the inlet of the Schreiner lens the
16 difference to the pressure at the exit of the lens becomes larger and therefore particles are accelerated to
17 higher velocities in the last aperture of the lens, thus particle flight times between the two detection
18 lasers decrease.

19 Similar measurements for the Liu lens were already presented in the literature (Schneider et al. (2006)).
20 There the velocities for particles with a diameter of 40 nm to 1000 nm were determined for a pressure
21 range from 1000 mbar to 200 mbar which corresponds to lens pressures of 1.6 mbar to 0.56 mbar.
22 Particle velocities are in the range of 200 m/s for 40 nm particles at 1000 mbar ambient pressure to
23 40 m/s for 1000 nm particles at 200 mbar.

24 Particle velocities measured in different aerosol mass spectrometers are shown in Figure 6. Due to the

1 low pressure difference between the inlet and exit of the Liu lens (deployed in the Aerodyne Aerosol
2 Mass Spectrometer and the SPLAT-MS by Imre and co-workers) particles reach velocities up to
3 150 m/s only. The Schreiner lens (deployed in our SPLAT and PALMS) works with a higher pressure
4 difference, which is also variable, because the inlet pressure in our instrument can be regulated between
5 50 mbar and 250 mbar. Therefore particles are accelerated to higher velocities compared to the Liu
6 design. The highest velocities, up to 420 m/s are achieved with a capillary inlet (deployed in old
7 versions of ATOFMS and SPLAT and also LAMPAS 2).

8 The different particle velocities have to be taken into account when discussing effects like evaporation
9 of volatile components due to long residence times in a high vacuum environment. In addition to this,
10 the choice of the ionization laser and the necessary trigger scheme can be affected by the particle
11 velocity when designing a new single particle laser ablation instrument. Both effects are discussed in
12 detail by Hinz and Spengler (2007).

13

14 **Detection Efficiency**

15 A disadvantage of the aerodynamic lens design by J. Schreiner is the variation of the particle beam
16 diameter with lens pressure and particle size. Figure 7 shows the pressure dependence of the particle
17 beam width for 800 nm particles. These particles are focused to a beam diameter (standard deviation of
18 Gaussian fit) of 0.14 mm at 250 mbar at the position of the second photomultiplier, which is located 76
19 mm behind the exit of the aerodynamic lens. With these values a solid angle of $1.07 \cdot 10^{-5}$ sr can be
20 calculated, which is comparable with the value of $4.4 \cdot 10^{-6}$ sr presented by Huffman et al. (2005) for the
21 Schreiner lens in a summary of particle beam width measurements. At lower pressures the beam
22 becomes broader (0.35 mm at 200 mbar and 0.49 mm at 150 mbar) and as a consequence the detection
23 efficiency decreases. The detection efficiency is defined as the percentage of sized particles compared
24 to the particles which enter the instrument through the critical orifice over the detectable size range of

1 the instrument. Therefore it is composed of the transmission efficiency of the aerodynamic lens, the
2 sizing efficiency, dependent on the cross section of the particle beam and the detection laser beam and
3 an enrichment factor for the Schreiner lens setup.

4 With the Schreiner lens, optimum focusing properties for different particle sizes are achieved at
5 different pressures. This can clearly be seen in Figure 8 where detection efficiencies for different
6 particles sizes at various pressures are shown. With the SMPS systems the particle concentration at the
7 inlet can be measured only up to 800 nm, therefore an APS and an OPC were used for larger particles.
8 When increasing the particle size from 300 nm to 800 nm the maximum detection efficiency is shifted
9 to higher pressures. This can be explained by the differences in the particle stopping distance. Larger
10 particles need higher pressures in the aerodynamic lens to influence their trajectories in such a way that
11 they do not impact on the apertures. For larger particles no distinct detection efficiency maximum can
12 be found within the pressure range of the measurement.

13 Figure 9 shows a comparative measurement for 800 nm particles with three reference techniques. All
14 three measurements agree within the uncertainty of measurement, which is shown exemplarily for the
15 APS measurement at 190 mbar. There the absolute error of the detection efficiency is $\pm 2.5\%$ with the
16 largest fraction emerging from the 10% relative error for the particle concentration measured with the
17 APS instrument. In Figure 7 it was shown that 800 nm particles are focused best at 250 mbar. This
18 result is in agreement with the data from Figure 8, where at 220 mbar the detection efficiency for
19 800 nm particles is still increasing.

20 In the PhD thesis by P. Budz (2002) from J. Schreiner's group at the MPI Heidelberg a lens with
21 exactly the same aperture layout as ours has been characterized. At 87 mm from the exit of the
22 aerodynamic lens a beam width of 0.5 - 2.5 mm for particles sizes between 0.3 μm and 5.0 μm at
23 pressures from 100 mbar to 200 mbar was found. The resulting solid angle is $1.04 \cdot 10^{-4}$ sr to $2.60 \cdot 10^{-3}$
24 sr. For defining the beam width they used the "two standard deviation" definition. The beam width

1 values are close to those found in Figure 7, where the beam width is between 0.14 mm and 0.49 mm.
2 With a width of the detection laser focus of $\sim 190 \mu\text{m}$, it can easily be seen that the detection efficiency
3 can not exceed 35% due to the fact that there is a limited overlap between the detection laser beam and
4 the particle beam generated by the aerodynamic lens. Other reasons reducing the detection efficiency
5 are the transmission efficiency of the aerodynamic lens and other transmission losses of the inlet
6 system.

7 Similar measurements of the detection efficiency were performed using the Liu aerodynamic lens as an
8 inlet for our SPLAT instrument. Figure 10 shows the detection efficiency measured for different
9 particle sizes from 300 nm to 2000 nm. For 500 nm and 600 nm particles the maximum detection
10 efficiencies are $> 50\%$. This is a factor of 1.6 higher maximum detection efficiency compared to the
11 Schreiner lens setup for 800 nm particles at 250 mbar. A similar factor between the two inlet
12 configurations was found when ambient air was sampled over a period of 4 h and the mean detection
13 efficiency over the whole size range was calculated. With the Schreiner lens setup at 90 mbar a mean
14 detection efficiency of 2.0% was achieved, while with the Liu lens setup this value increased to 7.3%.

15 The shape of the detection efficiency profile for the Liu lens in Figure 10 is caused by two limitations.
16 For particle sizes smaller than 300 nm the scattered light intensity is so small that it can not be
17 distinguished from the background radiation in our optical detection setup. Therefore the detection
18 efficiency decreases for particles smaller than 400 nm, although the Liu lens has a transmission of close
19 to 100% for this particle size (Liu et al. (2007)). Variations in particle beam width are unlikely to be
20 responsible for the strong decrease in detection efficiency for small particles because only factors of up
21 to 5 for solid angles for different particles sizes focused with the Liu lens can be found in the study by
22 Huffman et al. (2005). For large particles the detection efficiency decreases because the Liu lens has
23 only a very low transmission for particles larger than 800 nm (Liu et al. (2007)). These two limitations
24 account for the fact that the working range of the SPLAT instrument and the Liu lens do not match

1 perfectly. Nevertheless the mean detection efficiency for the Liu lens setup is still higher than for the
2 Schreiner lens setup.

3 As a consequence, in future field applications the Schreiner lens will be used in our SPLAT instrument
4 which is able to detect particles with diameters larger than 300 nm, if one is preferentially interested in
5 the chemical composition of particles larger than 1000 nm. For these supermicron particles the
6 detection efficiency of our instrument with the Schreiner lens is larger compared to the Liu lens setup.
7 For the submicron particles down to 300 nm the Liu lens is favored especially at low particle
8 concentrations because in this size region the Liu lens setup is more efficient. At the moment the
9 pressure controlled Schreiner lens design is favored for aircraft based measurements because the
10 measurements are not influenced by variations in ambient pressure. But work on the implementation of
11 a pressure control for the Liu lens and characterization of the transmission has begun in our group.

12

13 **Ablation of Single Particles**

14 The ablation laser evaporates and ionizes the particles at a point 105 mm behind the exit of the
15 aerodynamic lens and 29 mm behind the second detection laser beam. Beam propagation of the
16 ablation laser beam is parallel to the second detection laser beam. Alignment of the ablation laser is
17 achieved by horizontal movement of the laser beam perpendicular to the particle beam and variation of
18 the laser trigger timing which corresponds to a movement in direction of particle beam propagation as
19 described above. Figure 11 shows the result of a screening of the cross section between particle beam
20 and ablation laser beam. Ablation of particles producing a mass spectrum with one or more signals
21 larger than 10% of the maximum signal intensity are counted as hit particles. Maximum hit rates (ratio
22 of hit particles to sized particles) of 94% can be obtained, which results in a maximum overall
23 efficiency (detection efficiency * hit rate) of ~ 30% for 800 nm particles at 250 mbar in the Schreiner
24 lens setup. From the screening plot in Figure 11 the size of the ionizing laser focus can be derived as

1 300 μm x 550 μm . These dimensions are in good agreement with the focus dimensions on
2 photographic paper which can be seen on the right side of Figure 11.
3 This efficiency is valid only for one particle size at one inlet pressure. To be able to compare the
4 overall efficiency with those of other instruments, measurements with ambient aerosol concentrations
5 were performed. Ambient air was sampled over a period of four hours. The number of hit particles was
6 compared to the ambient particle concentration determined with an OPC. The measurements showed
7 overall efficiencies of 1.9% with the Schreiner lens setup. Because hit rates for the Liu lens setup do
8 not differ from the Schreiner lens setup the overall efficiency for the Liu lens setup is 6.9%. Table 3
9 shows detection efficiencies and hit rates of different single particle laser ablation instruments from our
10 measurements and from the literature. The detection efficiency and the hit rate of our instrument as
11 well as the detectable size range are comparable to those of other instruments but could be improved
12 further by integrating elliptical mirrors for enhancing the scattered light signal intensity and by
13 optimizing the overlap between the particle beam and the sizing lasers. For both optimizations a major
14 redesign of the recipient is necessary.

15

16 **Characterization of the Mass Spectrometer**

17 The mass spectrometer used in the SPLAT instrument is a bipolar time-of-flight mass spectrometer
18 equipped with reflectrons. The mass resolution for both polarities is 230 at m/z 36. The resolution is
19 sufficient to separate integer masses over a broad mass range. The mass accuracy is ± 0.20 at m/z 36
20 and ± 0.33 at m/z 50. With these values it is possible to work with one mass calibration up to m/z 100,
21 which is often sufficient due to intense fragmentation in our mass spectra (see sample field data). If
22 spectra with m/z values beyond 100 are evaluated a mass calibration has to be carried out for every
23 single particle spectrum. Different starting energies of the ions due to excess energy during the ablation
24 process are the main reason for variations in the mass accuracy.

1

2 **Sample field data**

3 To demonstrate the capabilities of our SPLAT instrument with respect to the chemical analysis of
4 single particles using the Schreiner lens in a typical field application with low number densities of
5 ambient particles, sample spectra are presented from the CLACE 6 (Cloud and Aerosol
6 Characterization Experiment) campaign, which took place in February/March 2007 at the High Alpine
7 Research Station Jungfraujoch, located in the Swiss Alps at an elevation of 3500 m asl. At an ambient
8 pressure of 620 mbar no problems with the HV supply or the excimer laser, which works with voltages
9 up to 12 kV, were observed.

10 The instrument sampled for 26 days with only small interruptions for realignment of the particle beam
11 and the laser beams. During that time mass spectra of 9777 background aerosol particles, 355 ice
12 residuals and 162 cloud condensation nuclei (one day experiment) with both polarities were recorded.
13 Mean particle concentrations above 300 nm were $2.6 \text{ particles cm}^{-3}$ at the total inlet, 0.3 cm^{-3} at the ice-
14 CVI (counterflow virtual impactor) which samples the ice residues only (Mertes et al. (2007)) and
15 7.6 cm^{-3} during the measurements of cloud condensation nuclei. Considering the low ambient particle
16 concentrations and the harsh environmental conditions, the results from the Jungfraujoch show that the
17 SPLAT instrument equipped with a suitably designed Schreiner lens as inlet can be deployed at field
18 campaigns even under difficult operating conditions. A more advanced and comprehensive analysis of
19 the data from the CLACE campaign will be presented elsewhere.

20 In Figure 12 mass spectra for two sample particles from the measurement of ambient aerosol at the
21 Jungfraujoch are presented, which are a representative for a particle class of the background aerosol
22 found during the CLACE 6 campaign. In the anionic spectrum on the left hand side mainly HSO_4 (m/z
23 97), C_2 (m/z 24) and HC_2 (m/z 25) are found. In the cationic spectrum C (m/z 12), C_2 (m/z 24) and C_3
24 (m/z 36) are prominent signals. In addition to this K (m/z 39), Si (m/z 28) and SiO (m/z 44) appear.

1 Other peaks may tentatively be identified as Fe (m/z 56), CaO (m/z 56), Ca (m/z 40) or NaOH (m/z
2 40). Therefore, this particle may be described as a mineral particle with sulfate and organic
3 components. At the lower part of Figure 12 the mass spectrum resulting from the raw data is shown. It
4 can be clearly seen that the resolution is high enough to generate stick spectra and that the stick spectra
5 contain the same information as the raw data spectra. Some small signals in the raw data spectra do not
6 appear in the stick spectra because their width is very small thus generating no significant intensity
7 when integrating over integer m/z values. The second particle also shows a strong signal for HSO₄ but
8 also nitrate can be found, NO₃ (m/z 62) and NO₂ (m/z 46). In the cationic spectrum the strongest
9 signals belong to K and NO (m/z 30). This particle is characterized best as a nitrate particle with
10 sulfate.

11 Hinz et al. (2005) presented a study on single particle analysis of ambient aerosol also measured at the
12 Jungfraujoch. They analyzed more than 2500 particles in the size range of 0.5 μm to 5.0 μm and found
13 mainly carbonaceous particles, carbon particles internally mixed with salts and/or secondary
14 components and mineral dust particles. A direct comparison of the mass spectra shows that our SPLAT
15 spectra are fragmented to a larger extent than the LAMPAS 2 spectra. In contrast to the LAMPAS 2
16 spectra we only rarely observe signals for ions with $m/z > 100$. Although the mass spectra from the
17 SPLAT and the LAMPAS 2 instrument differ in their individual composition, the particle classes
18 derived by classification with a clustering algorithm are similar for the Jungfraujoch measurements.

19 The main reasons why spectra from different single particle instruments cannot be compared directly
20 are the difference in wavelength and power density of the ablation laser. Table 4 shows a summary of
21 ionization wavelengths and power densities used with different instruments. As in our instrument,
22 193 nm is a very common wavelength for particle ablation, the commercial version of a single particle
23 instrument uses 266 nm, whereas the LAMPAS 2 works with a Nitrogen laser at 337 nm. Comparing
24 the photon energies shows that there is a factor of ~ 2 between the different wavelengths. So while one

1 compound might be ionized with two photons using 193 nm, at 377 nm already four photons are
2 needed.

3 Another important aspect is the absorption cross section at the different wavelengths applied in single
4 particle mass spectrometry. An example discussed by Murphy (2007) is sulfuric acid associated with
5 water. At 193 nm a higher energy density is necessary to produce ions from sulfuric acid compared to
6 other species that are easier to ionize. At 248 nm it was not possible at all to get spectra from pure
7 sulfuric acid. Concluding this discussion the author claims that there is a need for a further comparison
8 between different single particle mass spectra in laboratory experiments but also during field
9 campaigns. First results of such intercomparisons are presented by Hinz et al. (2006).

10 Figure 13 shows a part of the cationic mass spectrum from a single particle containing lead measured
11 during the CLACE 6 campaign in February/March 2007 at the Jungfraujoch, Switzerland. Clearly the
12 isotopic pattern of lead (m/z 204, 206, 207, 208) can be seen with a resolution sufficient to separate
13 integer masses. In a similar way, via the isotopic pattern of mercury, Murphy et al. (1998) discovered
14 with single particle laser ablation mass spectrometry that mercury is most common in particles just
15 above the tropopause region. Murphy et al. (2007) presented a study on lead distribution in single
16 atmospheric particles and found in measurements at several sites - amongst others also at the
17 Jungfraujoch - that more than 5% of the particles contained lead. In our samples we found 9% of the
18 ambient aerosol particles contained lead which is in agreement with the findings by Murphy et al.
19 Further investigations especially on the role of lead in ice nucleation will be discussed in a forthcoming
20 publication.

21

22 **Conclusion and Outlook**

23 In this paper we describe the setup and characterization of our Single Particle Laser Ablation Time-of-

1 flight mass spectrometer (SPLAT) equipped with two different aerodynamic lenses. Using the
2 Schreiner lens we achieve a mean detection efficiency of 2.0 % in the size range of 300 nm to 3000 nm.
3 The lens is actively pumped and therefore well suited for airborne measurements. The pressure at the
4 inlet can be regulated between 50 mbar and 250 mbar. The beam width of the focused particle beam
5 and thus the detection efficiency of our SPLAT instrument are strongly dependent of the particle size
6 and the pressure at the inlet of the aerodynamic lens.

7 The mean detection efficiency of our instrument when equipped with the Liu lens is 7.3% in the size
8 range of 300 nm to 2000 nm. The higher detection efficiency shows that the beam width of the Liu lens
9 is smaller compared to the Schreiner lens. However, the operating regime of the Liu lens and our
10 instrument do not match perfectly. The Liu lens focuses particles best in the size range between 80 nm
11 and 800 nm but our instrument currently detects only particles that are larger than 300 nm. To improve
12 this issue the lower size detection limit has to be decreased. This can be achieved by use of elliptical
13 mirrors for the particle detection (Su et al. (2004), Zelenyuk and Imre (2005)) but requires a major
14 redesign of our setup. We will apply elliptical mirrors in a new instrument for airborne single particle
15 analysis that is currently under development. For aircraft deployment the Liu lens will be modified so
16 that it can be actively pumped and the pressure in front of the aerodynamic lens is held constant.

17 The mass spectrometer of our SPLAT instrument shows a resolution high enough to separate single
18 masses up to the size region of m/z 200, enabling us to investigate the chemical composition of
19 individual aerosol particles. Data analysis is done on the basis of integer m/z values. Data interpretation
20 for ensembles of single particle mass spectra is done using clustering techniques. At the moment we
21 use a k-means algorithm. Further interpretation using other algorithms (e.g. fuzzy c-means, ART2A)
22 for data evaluation and classification will be performed. Finally, in the future, results from our
23 instrument will be compared to other single particle instruments in the laboratory and in the field.

24

1 **Acknowledgements**

2 We thank Jochen Schreiner from the Max Planck Institute of Nuclear Physics in Heidelberg, Germany,
3 for the development of the aerodynamic lens which was implemented in our aerosol mass spectrometer
4 and Thomas Böttger for supporting the development of the SPLAT instrument.

5 Financial support of the German Science Foundation DFG within the Collaborative Research Centre
6 641 “The Tropospheric Ice Phase” and the Research Training Group 826 “Trace Analysis of Elemental
7 Species“ as well as internal funding by Max Planck Institute for Chemistry is gratefully acknowledged.

8 M. Brands wants to thank the federal state of Rheinland Pfalz for funding within the Excellence Cluster
9 “Geocycles”.

1 **References**

2

3 Bahreini, R., Jimenez, J. L., Wang, J., Flagan, R. C., Seinfeld, J. H., Jayne, J. T., and Worsnop, D. R.
4 (2003). Aircraft-based aerosol size and composition measurements during ACE-Asia using an
5 Aerodyne aerosol mass spectrometer. *J. Geophys. Res.* 108(D23):8645, doi: 10.1029/2002JD003226.

6

7 Budz, P. (2002). Bildung und Untersuchung stratosphärisch relevanter fester Phasen in der AIDA
8 Aerosolkammer. PhD work, University of Heidelberg.

9

10 Canagaratna, M. R., Jayne, J. T., Jimenez, J. L., Allan, J. D., Alfarra, M. R., Zhang, Q., Onasch, T. B.,
11 Drewnick, F., Coe, H., Middlebrook, A., Delia, A., Williams, L. R., Trimborn, A., M., Northway, M.
12 J., DeCarlo, P. F., Kolb, C. E., Davidovits, P., and Worsnop, D. R. (2007). Chemical and microphysical
13 characterization of ambient aerosols with the Aerodyne aerosol mass spectrometer. *Mass Spec. Rev.*
14 26:185-222.

15

16 Cziczo, D. J., DeMott, P. J., Brock, C., Hudson, P. K., Jesse, B., Kreidenweiss, S. M., Prenni, A. J.,
17 Schreiner, J., Thomson, D. S., and Murphy, D. M. (2003). A method for single particle mass
18 spectrometry of ice nuclei. *Aerosol Sci. Technol.* 37:460-470.

19

20 Cziczo, D. J., Murphy, D. M., Hudson, P. K., and Thomson, D. S. (2004). Single particle measurement
21 of the chemical composition of cirrus ice residue during CRYSTAL-FACE. *J. Geophys. Res.*
22 109(D04201), doi: 10.1029/2003JD004032.

23

24 Cziczo, D. J., Thomson, D. S., Thompson, T. L., DeMott, P. J., and Murphy, D. M. (2006). Particle

1 analysis by laser mass spectrometry (PALMS) studies of ice nuclei and other low number density
2 particles. *Int. J. Mass Spec.* 258:21-29.

3

4 DeCarlo, P. F., Slowik, J. G., Worsnop, D. R., Davidovits, P., and Jimenez, J. L. (2004). Particle
5 Morphology and Density Characterization by Combined Mobility and Aerodynamic Diameter
6 Measurements. Part 1: Theory. *Aerosol Sci. Technol.* 38:1185-1205, doi: 10.1080/027868290903907.

7

8 DeCarlo, P. F., Kimmel, J. R., Trimborn, A., Northway, M. J., Jayne, J. T., Aiken, A. C., Gonin, M.,
9 Fuhrer, K., Horvath, T., Docherty, K. S., Worsnop, D. R., and Jimenez, J. L. (2006). Field-deployable,
10 high-resolution, time-of-flight aerosol mass spectrometer. *Anal. Chem.* 78:8281-8289.

11

12 Gard, E., Mayer, J. E., Morrical, B. D., Dienes, T., Fergenson, D. P., and Prather, K. A. (1997). Real-
13 Time Analysis of Individual Atmospheric Aerosol Particles: Design and Performance of a Portable
14 ATOFMS. *Anal. Chem.* 69:4083-4091.

15

16 Haas, G. J. R., and Kalcher, K. (1996). Fast Recording Software with Automatic Mass Calibration for
17 the Laser-Microprobe-Mass-Analyzer LAMMA-500. *Computers Chem.* 20:347-352.

18

19 Hinz, K.-P., Kaufmann, R., and Spengler, B. (1996). Simultaneous detection of positive and negative
20 ions from single airborne particles by real-time laser mass spectrometry. *Aerosol Sci. Technol.* 24:233-
21 242.

22

23 Hinz, K.-P., Trimborn, A., Weingartner, E., Henning, S., Baltensberger, U., and Spengler, B. (2005).
24 Aerosol single particle composition at the Jungfraujoch. *J. Aerosol Sci.* 36:123-145.

1
2
3
4
5
6
7
8
9
10
11
12
13
14
15
16
17
18
19
20
21
22
23
24

Hinz, K.-P., Erdmann, N., Grüning, C., and Spengler, B. (2006). Comparative parallel characterization of particle populations with two mass spectrometric systems LAMPAS 2 and SPASS. *Int. J. Mass Spec.* 258:151-166.

Hinz, K.-P., and Spengler, B. (2007). Instrumentation, data evaluation and quantification in on-line aerosol mass spectrometry. *J. Mass Spec.* 42:843-860.

Huffman, J. A., Jayne, J. T., Drewnick, F., Aiken, A. C., Onasch, T., Worsnop, D. R., and Jimenez, J. L. (2005). Design, Modelling, Optimization, and Experimental Tests of a Particle Beam Width Probe for the Aerodyne Aerosol Mass Spectrometer. *Aerosol Sci. Technol.* 39:1143-1163, doi: 10.1080/02786820500423782.

Kleimann, L. I., Daum, P. H., Lee, Y.-N., Senum, G. I., Springston, S. R., Wang, J., Berkowitz, C., Hubbe, J., Zaveri, R. A., Brechtel, F. J., Jayne, J., Onasch, T. B., and Worsnop, D. (2007). Aircraft observations of aerosol composition and ageing in New England and Mid-Atlantic States during the summer 2002 New England Air Quality Study field campaign. *J. Geophys. Res.* 112(D09310), doi: 10.1029/2006JD007786.

Liu, P. S. K., Deng, R., Smith, K. A., Williams, L. R., Jayne, J. T., Canagaratna, M. R., Moore, K., Onasch, T. B., Worsnop, D. R., and Deshler, T. (2007). Transmission Efficiency of an Aerodynamic Focusing Lens System: Comparison of Model Calculations and Laboratory Measurements for the Aerodyne Aerosol Mass Spectrometer. *Aerosol Sci. Technol.* 41:721-733, doi: 10.1080/02786820701422278.

1

2 Mertes, S., Verheggen, B., Walter, S., Connolly, P., Ebert, M., Schneider, J., Bower, K. N., Cozic, J.,
3 Weinbruch, S., Baltensperger, U., and Weingartner, E. (2007). Counterflow virtual impact or based
4 collection of small ice particles in mixed-phase clouds for the physico-chemical characterization of
5 tropospheric ice nuclei: Sampler description and first case study. *Aerosol Sci. Technol.* 41:848-864.

6

7 Murphy, D. M., Thomson, D. S., and Mahoney, M. J. (1998). In situ measurements of organics,
8 meteoritic material, mercury, and other elements in aerosols at 5 to 19 kilometers. *Science* 282:1664-
9 1669.

10

11 Murphy, D. M. (2007). The design of single particle laser mass spectrometers. *Mass Spec. Rev.* 26:150-
12 165.

13

14 Murphy, D. M., Hudson, P. K., Cziczo, D. J., Gallavardin, S., Froyd, K. D., Johnston, M. V.,
15 Middlebrook, A. M., Reinard, M. S., Thomson, D. S., Thornberry, T., and Wexler, A. S. (2007).
16 Distribution of lead in single atmospheric particles. *Atmos. Chem. Phys.*, 7:3195-3210.

17

18 Nash, D. G., Baer, T., and Johnston, M. V. (2006). Aerosol mass spectrometry: An introductory
19 review. *Int. J. Mass Spec.* 258:2-12.

20

21 Prather, K. A., Nordmeyer, T., and Salt, K. (1994). Real-time characterization of individual aerosol
22 particles using time-of-flight mass spectrometry. *Anal. Chem.* 66:1403-1407.

23

24 Schneider, J., Borrmann, S., Wollny, A. G., Bläsner, M., Mihalopoulos, N., Oikonomou, K., Sciare, J.,

1 Teller, A., Levin, Z., and Worsnop, D. R. (2004). Online mass spectrometric aerosol measurements
2 during the MINOS campaign (Crete, August 2001). *Atmos. Chem. Phys.* 4:65-80.

3

4 Schneider, J., Hings, S. S., Hock, B. N., Weimer, S., Borrmann, S., Fiebig, M., Petzold, A., Busen, R.,
5 and Karcher, B. (2006). Aircraft-based operation of an aerosol mass spectrometer: Measurements of
6 tropospheric aerosol composition. *J. Aerosol Sci.* 37:839-857.

7

8 Schoolcraft, T. A., Constable, G. S., Zhigilei, L. V, and Garrison, B. J. (2000). Molecular dynamics
9 simulation of the laser disintegration of aerosol particles. *Anal. Chem.* 72:5143-5150.

10

11 Schreiner, J., Schild, U., Voigt, C., and Mauersberger, K. (1999). Focussing of aerosols into a particle
12 beam at pressures from 10 to 150 torr. *Aerosol Sci. Technol.* 31:373-382.

13

14 Su, Y., Sipin, M. F., Furutani, H., and Prather, K. A. (2004). Development and characterization of an
15 aerosol time-of-flight mass spectrometer with increased detection efficiency. *Anal. Chem.* 76:712-719.

16

17 Thomson, D. S., Schein, M. E., and Murphy, D. M. (2000). Particle Analysis by Laser Mass
18 Spectrometry WB-57F Instrument Overview. *Aerosol Sci. Technol.* 33:153-169.

19

20 Trimborn, A., Hinz, K.-P., and Spengler, B. (2000). Online analysis of atmospheric particles with a
21 transportable laser mass spectrometer. *Aerosol Sci. Technol.* 33:191-201.

22

23 Wollny, A. G. (2002). Entwicklung eines bipolaren Flugzeitmassenspektrometers zur Analyse der
24 chemischen Zusammensetzung von individuellen Aerosolpartikeln. PhD work, University of Bonn.

1

- 2 Zelenyuk, A., and Imre, D. (2005). Single particle laser ablation time-of-flight mass spectrometer: An
3 introduction to SPLAT. *Aerosol Sci. Technol.* 39:554-568.

1 Figures

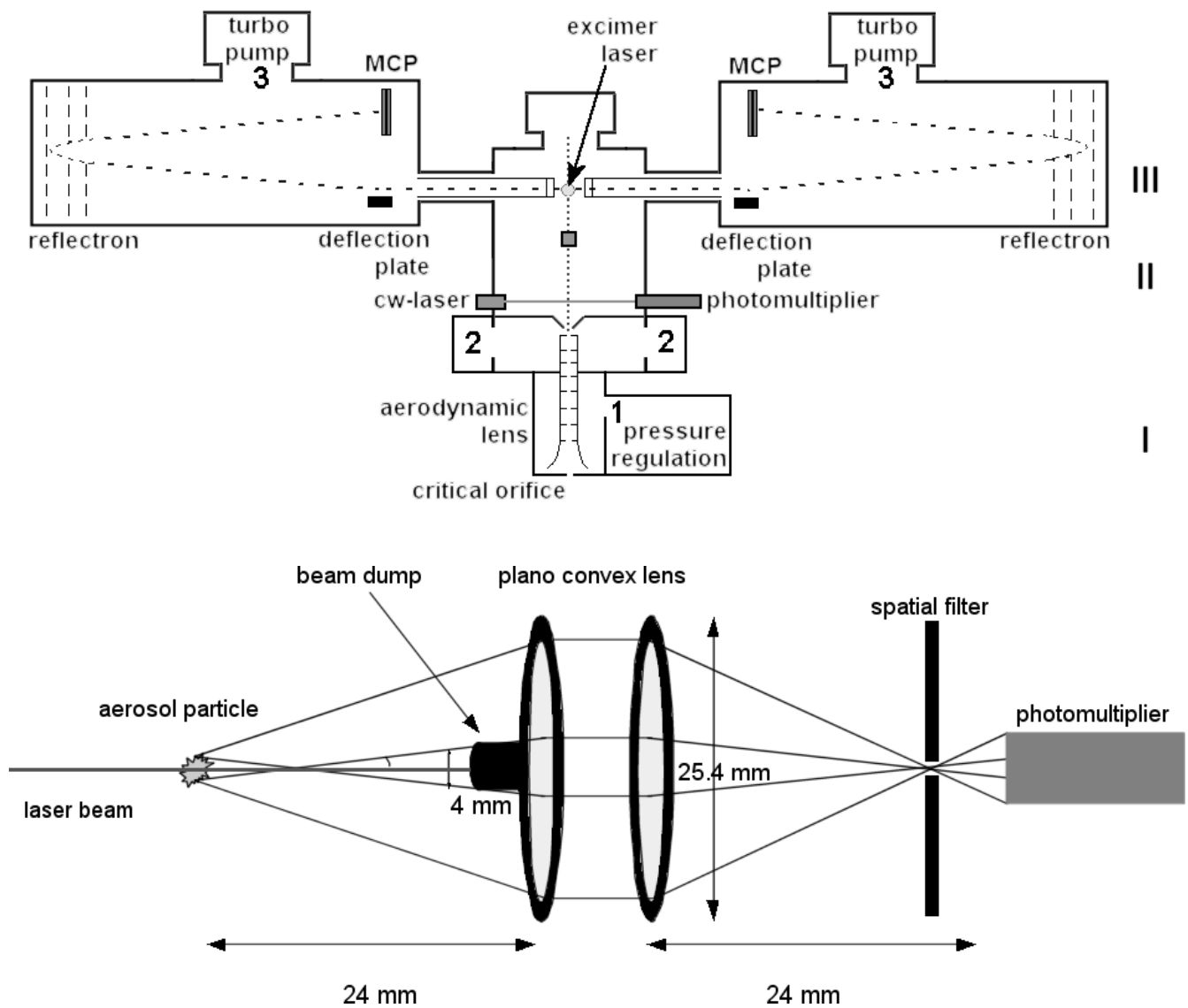


Figure 1: Upper part: sketch of the aerosol mass spectrometer SPLAT with three numbered sections of the instrument, which are the inlet system (I), the sizing region (II) and the chemical analysis of the particles (III); lower part: schematic drawing of detection optics. Scattered light is detected in forward direction.

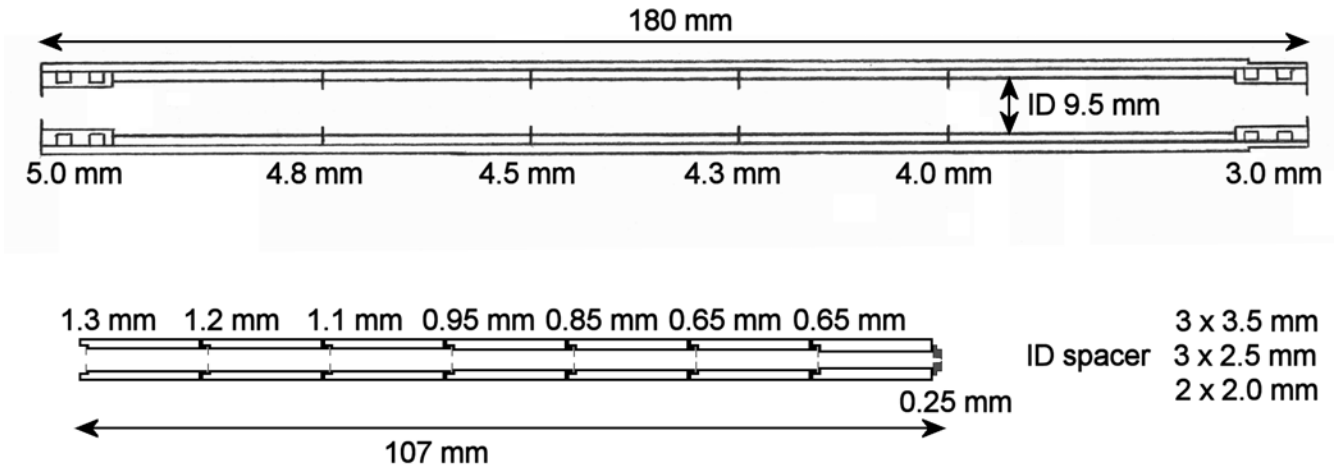


Figure 2: Comparison of Liu lens (upper part) and Schreiner lens (lower part). Flow direction is from left to right.

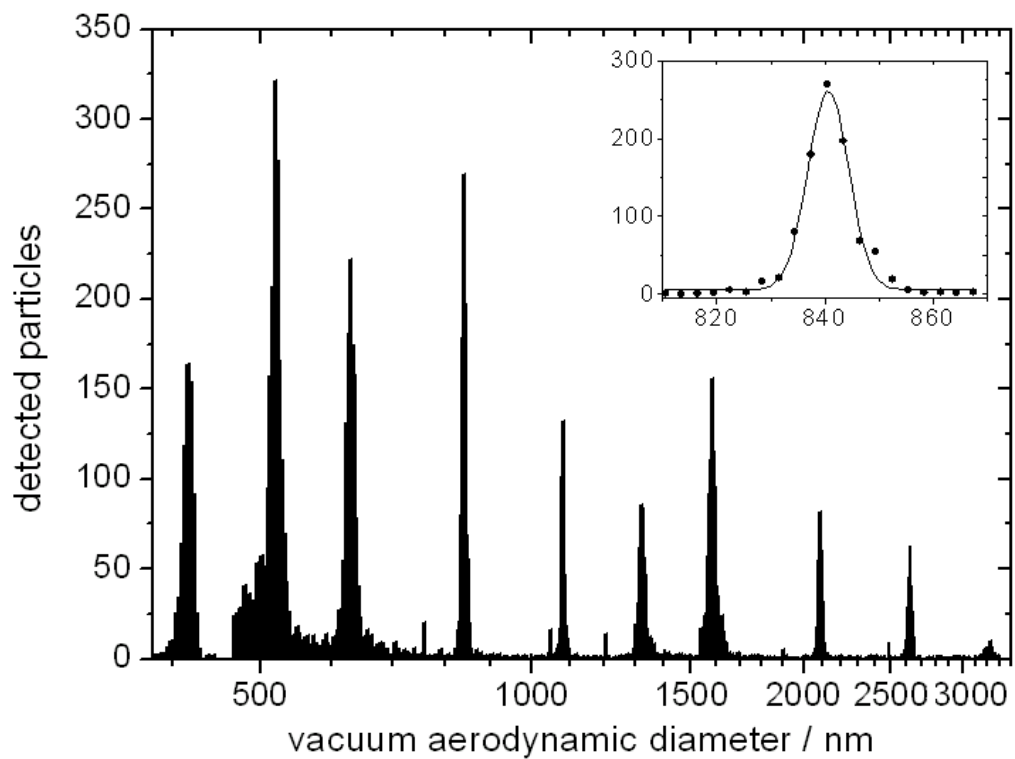


Figure 3: Particle histogram for PSL particles of different sizes focused with the Schreiner lens. The insert shows a Gaussian fit to the distribution for the 800 nm particles. The FWHM is 8 nm.

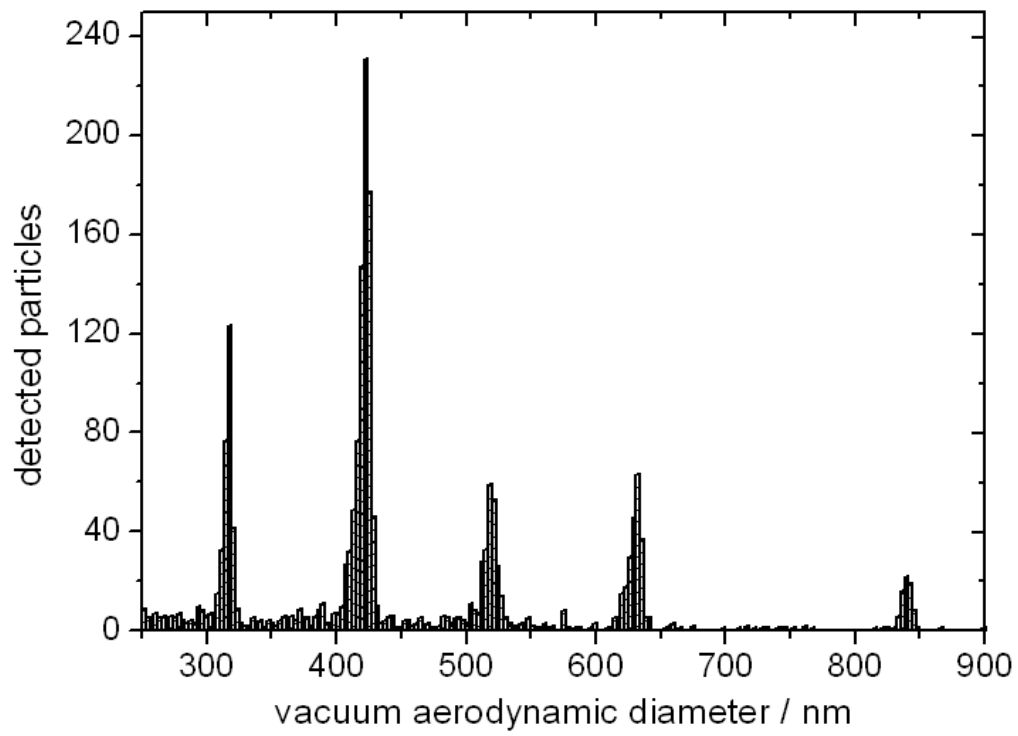
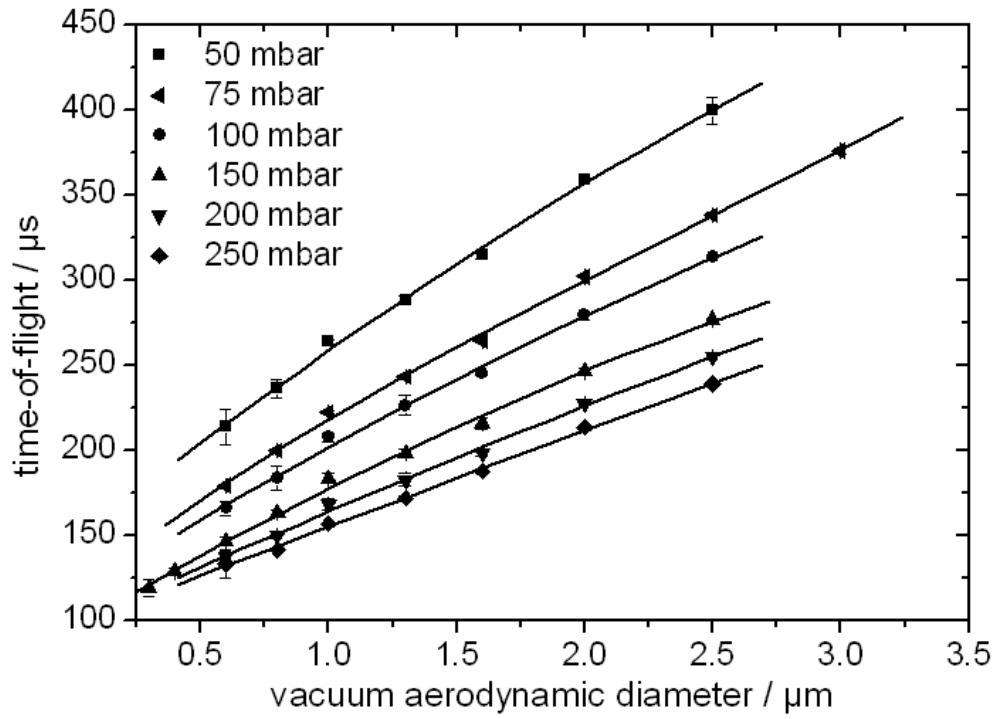


Figure 4: Particle histogram for PSL particles of different size focused with the Liu lens.



1

Figure 5: Correlation between the time-of-flight of particles and their vacuum aerodynamic size, measured at different pressures in front of the aerodynamic lens (Schreiner type).

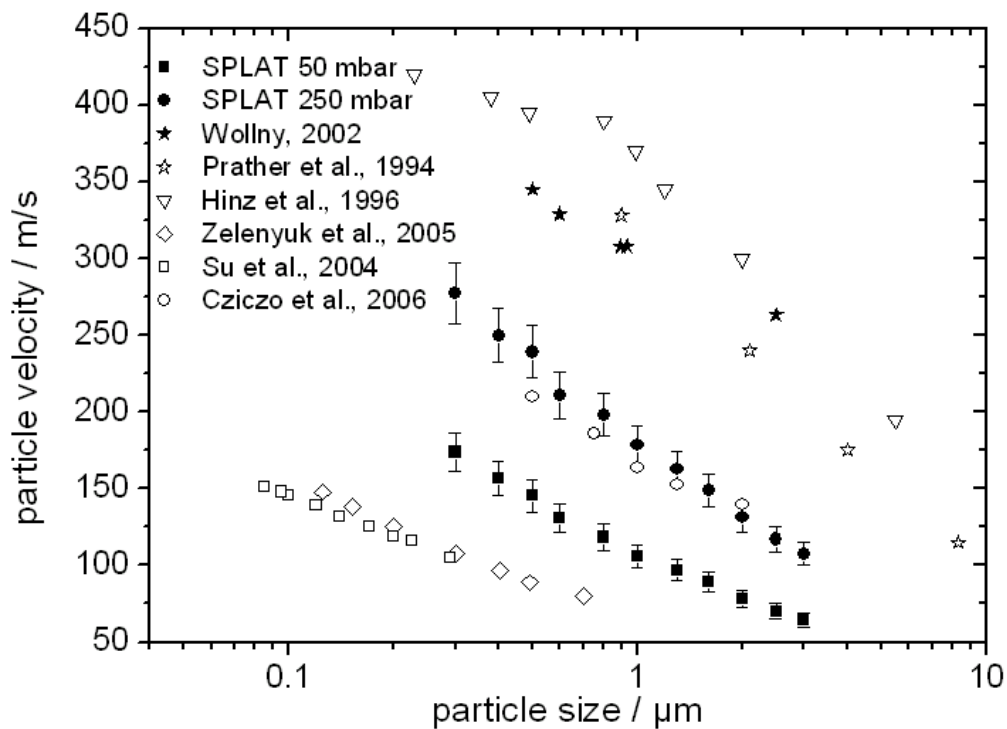


Figure 6: Particle velocities for different aerosol mass spectrometers. Particles focused with the Liu lens are the slowest with velocities up to 150 m/s. With the Schreiner lens particles become faster, 200 m/s up to 300 m/s depending on the inlet pressure of the lens. Capillary inlet systems provide the highest particle velocities up to 420 m/s. The error bars for our SPLAT instrument are dominated by the uncertainty in the distance between the two detection laser beams, which is set to be ± 2 mm.

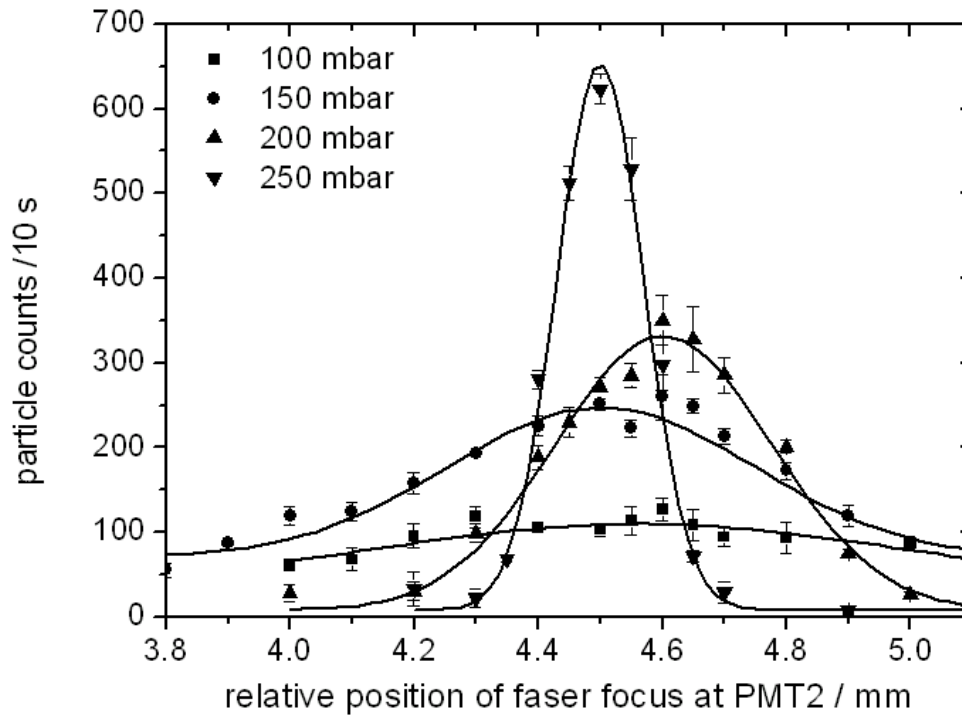


Figure 7: Beam width measurements for 800 nm PSL particles at different pressures in the Schreiner lens measured at the position of the second detection laser beam. Error bars show the standard deviation of several measurements.

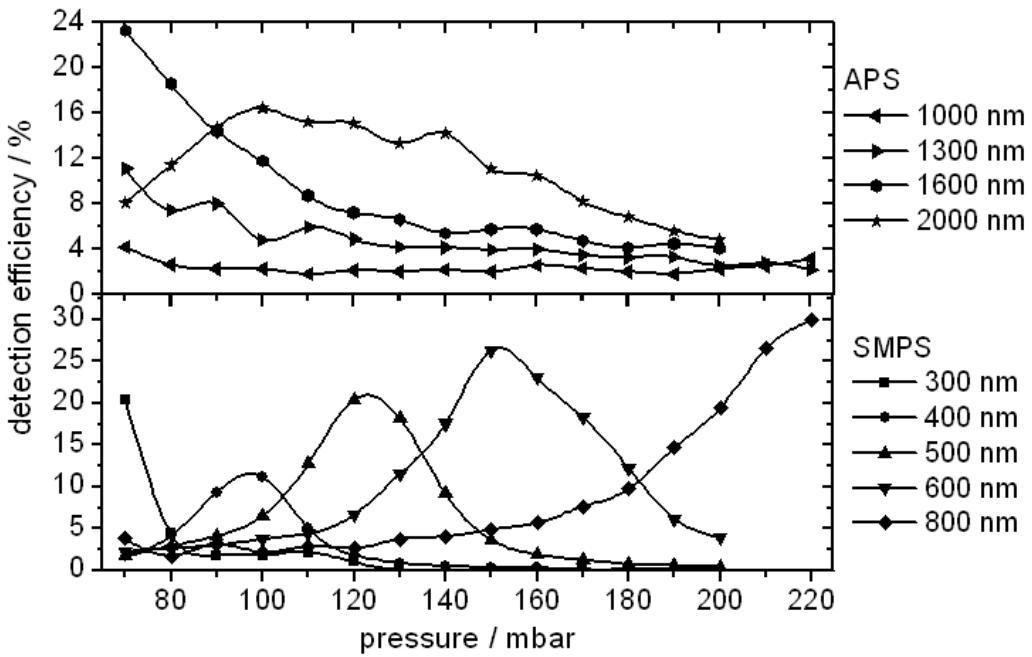


Figure 8: Detection efficiency for the SPLAT equipped with the Schreiner lens. Efficiencies were determined for 9 different sizes (from 300 nm to 2000 nm) at 14 different pressures. The 300 nm detection efficiencies are multiplied by 50 for better visibility.

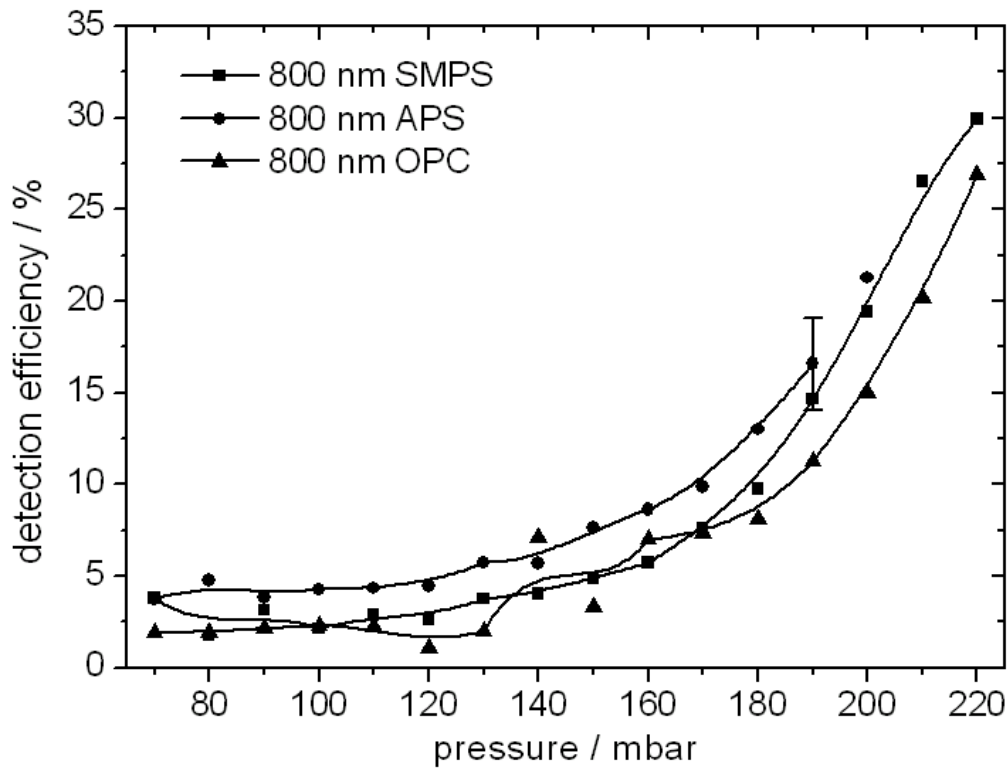


Figure 9: Detection efficiency for 800 nm particles focused with the Schreiner lens, measured with three different reference techniques (SMPS, APS, OPC).

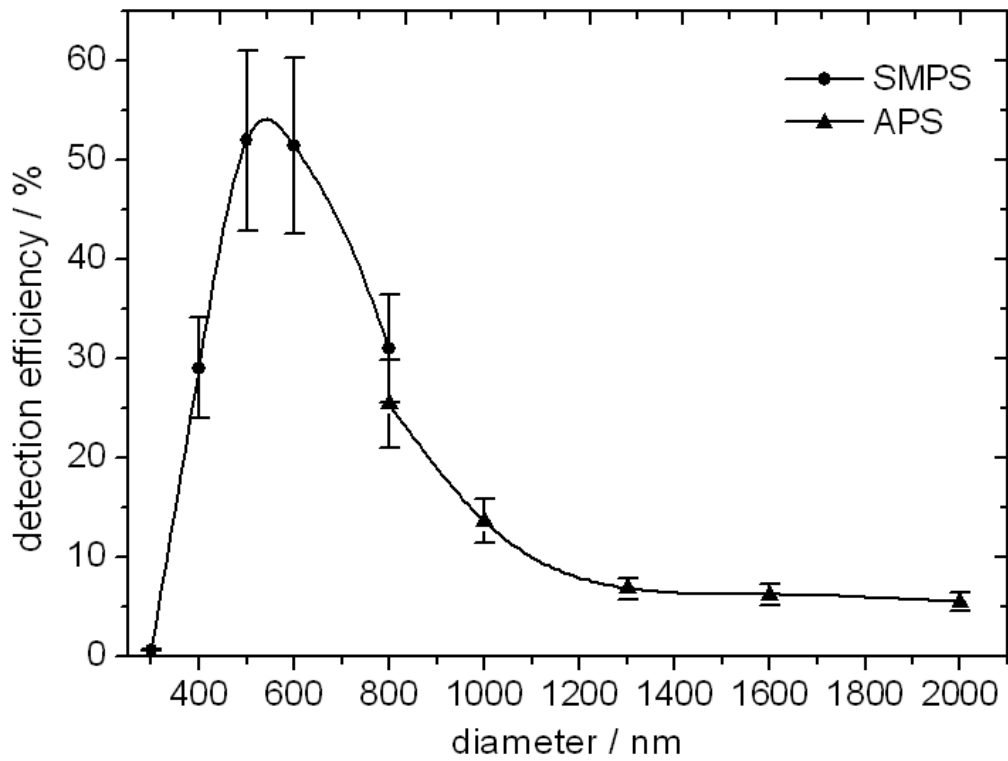


Figure 10: Detection efficiency for SPLAT equipped with the Liu lens. Concentrations of particles with sizes up to 800 nm were measured with a SMPS system. Starting with 800 nm an APS system was used. The error bars are dominated by the uncertainty of the measurement of the reference concentration (10% relative error for SMPS and APS).

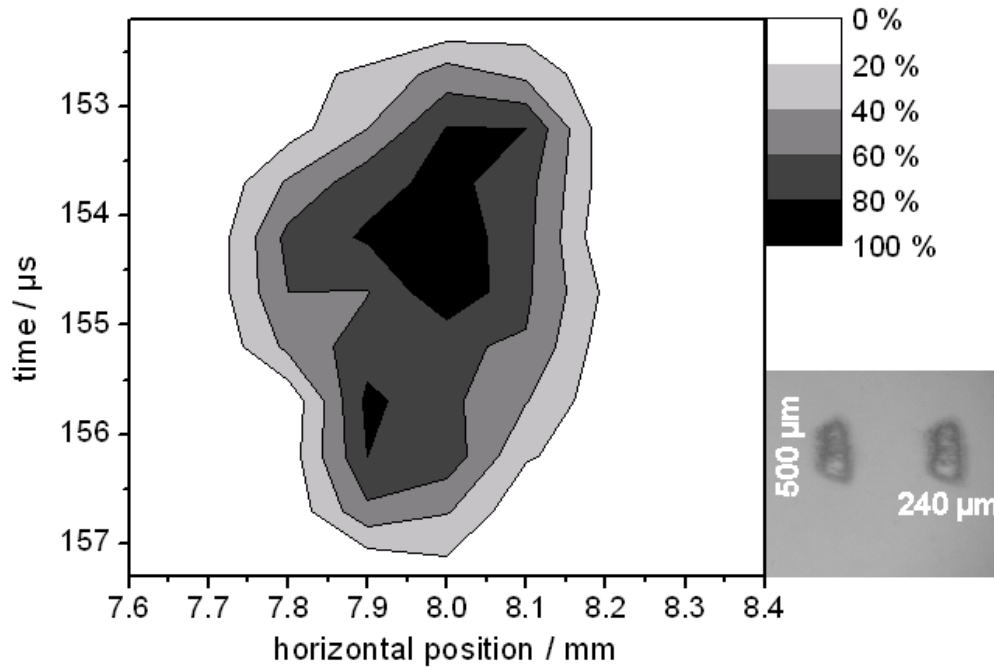


Figure 11: Hit rate of detected particles as a function of ablation laser focus position. By moving the excimer laser beam in the horizontal position and shifting the laser pulse in the time domain, which corresponds to a vertical movement, the cross section of the particle beam is screened. Hit rates above 80% can be achieved in the center region. On the right side a burn pattern from the laser focus on photographic paper is shown.

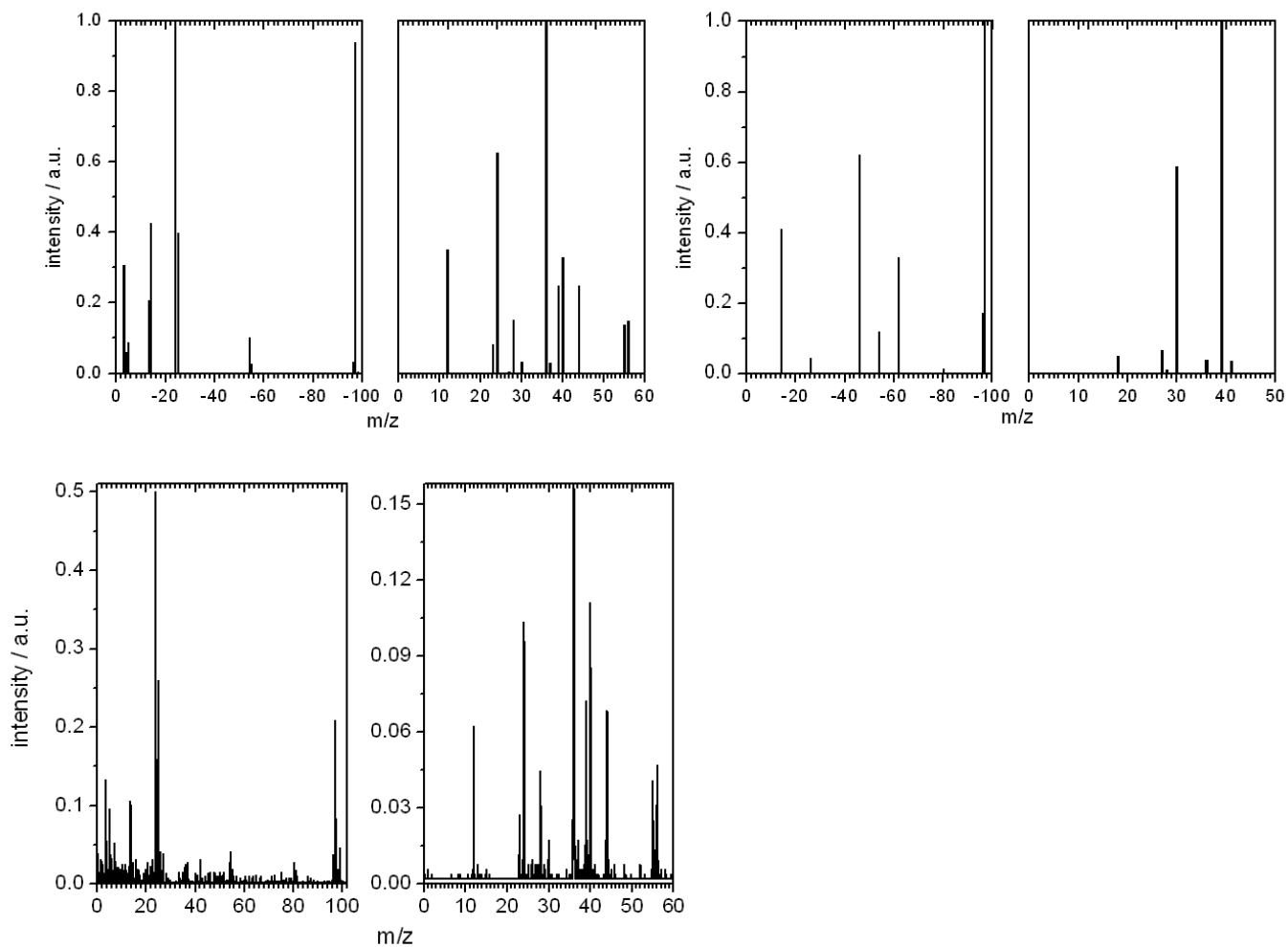


Figure 12: Upper part: Typical single particle stick mass spectra for ambient aerosol from the CLACE 6 campaign at the Jungfraujoch, Switzerland, in 2007. Left hand side: mineral particle with sulfate and organic compounds; right hand side: nitrate particle with sulfate. Lower part: mass spectrum from raw data of the first particle.

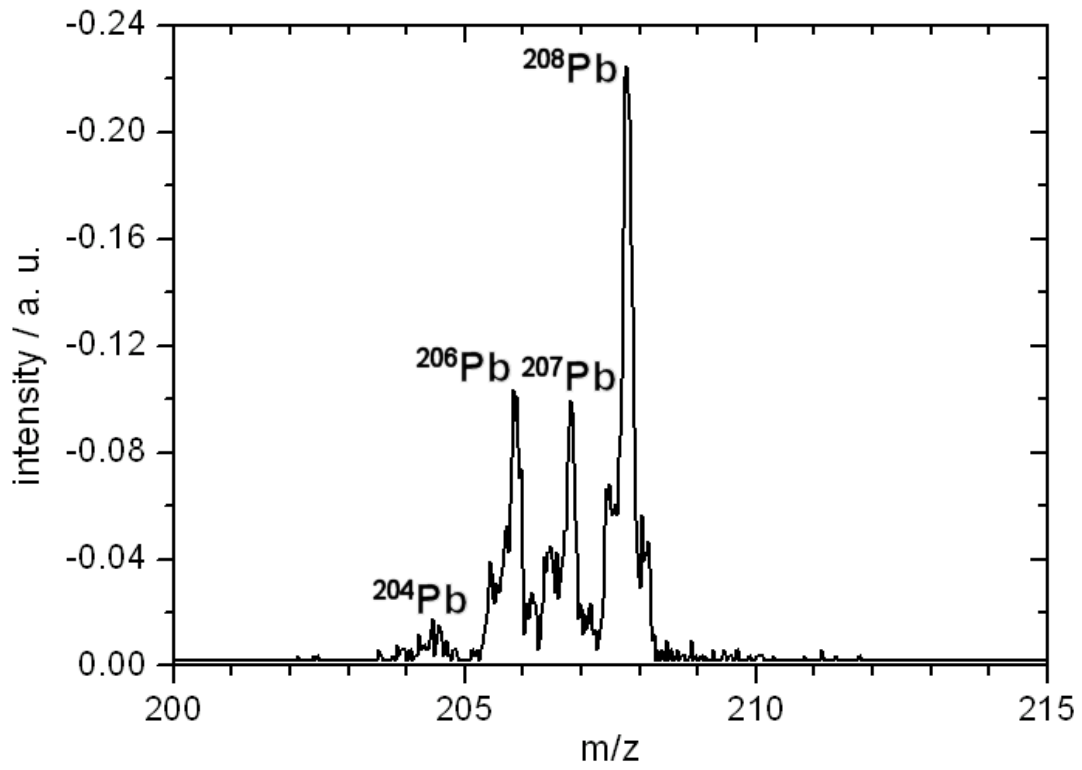


Figure 13: Isotopic pattern of lead from ambient aerosol, measured during the CLACE 6 campaign at the Jungfraujoch, Switzerland, in 2007.

Tables

Table 1: Different critical orifices used with the Schreiner lens at the SPLAT instrument and resulting flow into the instrument

diameter critical orifice μm	measured flow cm³/min
100	76.4 ± 0.1
150	190.1 ± 1.0
200	337.3 ± 1.0
250	518.1 ± 0.4

Table 2: Geometric diameter of PSL particles according to the manufacturer and calculated vacuum aerodynamic diameter. Also the vacuum aerodynamic diameter determined with the Schreiner and the Liu lens designs are shown. As errors the width of the Gaussian fit to the size distribution are given.

geom. particle size nm	vac. aerodyn. particle size nm	vac. aerodyn. particle size / Schreiner lens nm	vac. aerodyn. particle size / Liu lens nm
299 ± 6	314 ± 6		317 ± 5
404 ± 4	424 ± 4	418 ± 9	423 ± 7
499 ± 5	524 ± 5	520 ± 11	519 ± 9
596 ± 6	626 ± 6	631 ± 12	631 ± 8
799 ± 9	839 ± 9	841 ± 8	840 ± 7
1020 ± 22	1071 ± 23	1083 ± 8	
1300		1324 ± 19	
1600		1584 ± 22	
2003 ± 22	2103 ± 23	2089 ± 21	
2504 ± 25	2629 ± 26	2626 ± 23	
3063 ± 27	3216 ± 28	3221 ± 15	

Table 3: Detection efficiencies, hit rates and size ranges of different single particle laser ablation instruments. All instruments except the LAMPAS 2 work with an aerodynamic lens. LAMPAS 2 uses a capillary inlet.

instrument	lens type	reference	detection efficiency %	size range	hit rate %
SPLAT	Schreiner	this paper	2.0	300 nm – 3000 nm	94
SPLAT	Liu	this paper	7.3	300 nm – 1000 nm	94
SPLAT MS	Liu	Zelenyuk and Imre (2005)	1.0 (100 nm) > 10 (150 nm to 1000 nm)	50 nm – 1000 nm	30 - 90
ATOFMS	Liu	Su et al. (2004)	0.5 (95 nm) 47.4 (290 nm)	100 nm – 3000 nm	55 (95 nm) > 80 (> 120 nm)
PALMS	Liu	Cziczo et al. (2004)	10 (300 nm to 1000 nm)	150 nm – 2000 nm	95
PALMS	Schreiner	Cziczo et al. (2006)	0.22	150 nm – 2000 nm	> 90
LAMPAS 2	capillary	Trimborn et al. (2000) Hinz et al. (2005)	0.01 (500nm) 2.5 (1500 nm)	200 nm – 10 μm	

Table 4: Wavelength and energy density for the ablation laser beam used in different single particle laser ablation instruments.

instrument	reference	wavelength nm	photon energy eV	power density W/cm²
SPLAT	this paper	193	6.42	$1.6 \cdot 10^9$
SPLAT MS	Zelenyuk and Imre (2005)	193	6.42	$9.4 \cdot 10^8$
ATOFMS	Su et al. (2004)	266	4.66	$3 \cdot 10^8$
PALMS	Cziczo et al. (2003)	193	6.42	$2 - 5 \cdot 10^9$
LAMPAS 2	Trimborn et al. (2000)	377	3.29	10^9